Spark-Sintered W Alloys Doped with LaB_6†

Makoto TAKAHASHI*, Manabu TANAKA*, Takeo SHIRAI, Kenji IKEUCHI***, Masao USHIO*****

Abstract

LaB_6 doped W alloys were experimentally produced with the aim of developing new arc cathode materials by SPS. SPS is a new sintering method that applies a uniaxial stress and a pulse DC current to material powder to perform sintering. Alloys of three compositions, 25vol%LaB_6-W, 50vol%LaB_6-W, and 75vol%LaB_6-W were sintered at three different sintering temperatures, 1670 K, 1870 K, and 2070 K for a sintering time of 600 s. Pure W and pure LaB_6 powder was sintered in the same condition for comparison. At a sintering temperature of 2070 K, sintered blocks of high density were obtained for every composition. Produced alloys were metallographically analyzed, and it was found that in every alloy reactions of La and W occurred during sintering, and in 25vol%LaB_6-W alloys W_2B and W, in 50vol%LaB_6-W and 75vol%LaB_6-W alloys WB, LaB_4 and LaB_6 existed after sintering. In the 25vol%LaB_6-W alloy, La isolated by decomposition of LaB_6 was found to form complex oxides with W. Discharge tests of electrodes made of sintered alloys were performed. The consumption of electrodes of 50vol%LaB_6-W and 75vol%LaB_6-W was very rapid. Those alloys contained LaB_4 generated by reactions of W and LaB_6. The low melting point of LaB_4 might have a bad influence on the resistance of those alloys to high temperature. On the other hand, electrodes of 25vol%LaB_6-W showed rather good properties, in spite of the fact that 25vol%LaB_6-W alloys contained no LaB_6 after sintering. This alloy contained complex oxides of La and W, and its major component, W_2B, is a material of high melting point and low work function. These components might improve performance of the 25vol%LaB_6-W alloy as an electrode material.

KEY WORDS: (Tungsten) (Lanthanum) (Boride) (Complex Oxide) (Spark Plasma Sintering) (Arc Cathode) (Arc Discharge) (XRD) (EPMA) (TEM)

1. Introduction

Arc discharge with a hot cathode is a convenient way to produce plasma of high temperature and high energy density, and the field of its application to manufacturing is becoming steadily broader. To produce stable arc plasmas with desirable properties for various applications, it is necessary to use a cathode of easy arc ignition and high durability that warrants long lifetime with less change in performance. Increase of thermo-electron emittance of the cathode material produces a good improvement of arc ignition property, and long lifetime of the cathode because the cathode is able to provide plenty of electrons to maintain the discharge. Tungsten (W) alloy doped with thorium oxide (Thoria: ThO_2) is the most popular material for arc discharge electrodes[1]. Needless to say, W is the most refractory metal, and the addition of ThO_2, that is, a material of small work function and high melting point, improves thermo-electron emittance of this alloy. However, Thorium is a radioactive element and needs specially careful manipulation in the manufacturing process of the cathode material, and it is better to reduce the use of this element to keep a healthy environment. Moreover, there always exists a strong need for electrodes of longer lifetime and higher performance for advanced industrial applications. Therefore, development of new electrode materials that can replace ThO_2 doped W is a necessity today.

Lanthanum hexaboride (LaB_6) is purplish red material with a metallic luster, and is well-known for its low work function (2.3~2.6 eV) and high melting point (2993 K)[2,3]. It has been utilized in filaments for the electron guns of electron microscopes, and has the capacity to be a substitute for ThO_2 as an additive in arc cathode materials. But LaB_6 reacts with W and decomposes at high temperature.

† Received on June 1, 1998
* Research Associate
** Graduate Student (Presently at Furukawa Denko K. K.)
*** Professor

Transactions of JWRI is published by Joining and Welding Research Institute of Osaka University, Ibaraki, Osaka 567-0047, Japan.

Table 1 Compositions of starting materials prepared for SPS.

Electorode	LaB_6 content	
	wt%	at%
Pure W	0	0
25vol%LaB_6-W	8	7
50vol%LaB_6-W	20	18
75vol%LaB_6-W	43	40
100%LaB_6	100	100

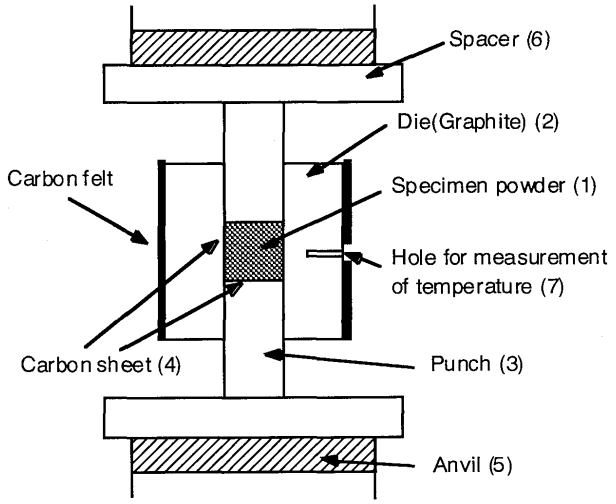

Fig. 1 Schematic diagram of the central part of the SPS apparatus.

Conventional sintering methods for W alloys keep the material over 3000 K for about 4000 s, so we cannot expect LaB_6 to be left in sintered alloys after such processing[4]. So in this study, we employed the spark-plasma-sintering method (SPS), for sintering of LaB_6 doped W alloys. SPS has proved to be capable of sintering of many materials in much shorter times at lower temperatures than other conventional sintering methods in many studies[5, 6, 7]. The alloys produced were examined for component phases and microstructure with X-ray diffraction (XRD), optical microscopy, scanning electron microscopy (SEM), and transmission electron microscopy (TEM). We performed discharge tests using electrodes produced from these alloys, and their performance as electrode materials was examined in relation to their microstructures.

2. Experimental Procedure

2. 1 Materials

Starting materials were W and LaB_6 powder. Mean diameters of these particles were 1.5 μm and 5.0 μm, respectively. Firstly these powders were mixed uniformly, and sintered by SPS under uniaxial stress of 50 MPa for a sintering time of 600 s at three different sintering temperatures, 1670 K, 1870 K, and 2070 K. Sintering was performed in a vacuum of 2 Pa. In **Table 1** are shown compositions of mixtures before sintering. Sintering of pure W and LaB_6 was also performed for comparison. The sintered compacts produced had the shape of cylinders of about 8 mm in height and 20 mm in diameter. The densities of these compacts were measured by Archimedes' method, and after that we performed metallographical analyses by several means and discharge tests.

2. 2 Spark plasma sintering

In the process of SPS, powder material is pressed under a uniaxial stress of several tens of MPa, and direct current, frequently switched on and off, is applied to the material to heat it[5]. Many studies have shown the capacity of SPS for speedy sintering at low temperature[6, 7], but it has not been well understood how this is achieved. Under SPS, plastic deformation of powder particles by high pressure enhances sintering. Some researchers say that intermittent current causes spark discharges among the powder particles and these discharges activate the surface of particles and assist rapid progress of sintering[8].

In this study, SPS of W-LaB_6 alloys was performed with an SPS apparatus SPS-1050 made by Sumitomo Coal Mining Co. In **Fig. 1** is shown a schematic diagram of the central part of the SPS apparatus. Specimen powder (1) was packed in the graphite die (2), and pressed by hydraulic press through punches of graphite (3). Specimen powder was separated from the die and punches by carbon sheets (4) in order to keep the die and punches from damages through reaction. Heating current was applied through the punches from anvils of the press (5) also, and punches themselves reached high temperature during sintering. To avoid damages of the anvils, plates of graphite (6) were inserted between punches and anvils. The illustrated part of the SPS apparatus was put in a chamber evacuated by a rotary pump and mechanical booster pump. To control the sintering temperature, we measured the temperature of the die by optical pyrometer. To measure temperature of the specimen as precise as possible, we made a small hole (7) in the wall of the die, and set the focus of pyrometer on the bottom of the hole. The measured temperature was fed back to the PID controller governing heating current. Specimens were heated at a rate of 100 ℃ / min., and after sintering, the specimen was left to cooling by heat conduction to anvils and by thermal radiation.

2. 3 Observation of microstructure

At first, sintered compacts were cut in the direction

of the axis of cylinder by a micro cutter. Sections of specimens were mechanically polished and etched by a solution of 15 g of potassium ferricyanide and 6 g of sodium hydroxide in 100 ml distilled water (Murakami's reagent)[9], and observed by optical microscopy. Point analyses by electron probe microanalyzer (EPMA) were applied on some specimens in order to determine the distributions of each component element. Component phases were identified by X-ray diffraction measurement (XRD) performed on etched sections. XRD was performed with the diffractometer method using Cu Kα characteristic X-ray. From these results, the phases observed by optical microscopy were identified to chemical compounds.

Transmission electron microscopy (TEM), electron diffraction (SAED) and energy dispersion X-ray spectroscopy (EDS) using TEM apparatus were performed on 25vol%LaB_6-W alloy sintered at 2070 K. The TEM specimens of that material were prepared by the following procedures. A thin plate was sectioned from the central part of the sintered compact, and the plate was ground to a thickness under 100 μm. Disks of 3 mm in diameter were cut from the plate, and shallow pits were made on the central parts of the disks with a dimple grinder. Argon atom milling was employed to finish thin foil specimens for TEM. TEM observation was performed with JEM-2010 FX microscope made by JEOL Co. at a beam accelerating voltage of 200 kV.

2. 4 Discharge tests

Discharge tests were performed for electrodes made from four alloys different in composition, 25vol%LaB_6-W, 50vol%LaB_6-W, 75vol%LaB_6-W, and pure LaB_6. All these alloys were sintered at 1870 K. The atmosphere for discharge tests was Ar at 2 MPa pressure. Other experimental conditions are tabulated in **Table 2**. Each test started with a discharge current of 10 A, and the current was increased step by step to 50 A. Next the current was decreased step by step to 10 A. The current was kept at each value for 600 s. In these experiments, we gave attention to two parameters; the range of fluctuation of the discharging voltage at each discharging current for evaluation of stability of arc discharge, and the difference between medians of discharging voltages at the same discharging current in the current increasing cycle and the decreasing cycle for evaluation of durability of electrodes. Electrodes made from 2wt%ThO_2-W and 2wt%La_2O_3-W (La_2O_3: lanthanum oxide) sintered with conventional non pressure Joule heating were tested in the same condition for comparison. For La_2O_3-W two different electrodes were tested: one was as-sintered material, and the other had received surface carburizing treatment.

After discharge tests, we checked the appearance of electrodes by optical microscopy to evaluate the damage electrodes had suffered during discharge tests.

Table 2 Experimental conditions of discharge tests.

	Discharging test A
Pressure	2 MPa
Atmosphere	Ar
Electrode diameter	ϕ3.2 mm
Electrode tip angle	60°
Arc gap	1 mm
Arc current	10→12→15→25→40→50 →40→30→25→15→12 →10A (changed step by step)
Operating time	600 s for every step

3. Results and Discussion

3. 1 Density of sintered blocks

In Table 3 are tabulated the change of density of sintered alloys with compositions and sintering temperature. 'Relative density' presented in the table is the ratio of the observed density of each alloy to the 'ideal density', (density calculated on the assumption that reaction between W and LaB_6 in the starting materials did not occur at all, and they were densely sintered without any pores). The relative density of alloys sintered at 2070 K exceeded 95% for all compositions. These results show that, by SPS it is possible to sinter W alloys at a sintering temperature lower by about 1000 K than conventional methods (e. g. non pressure Joule heating: with sintering temperature over 3000 K, and the sintering time of about 4000 s) in a very short sintering time.

Relative density exceeded 100% for 50vol%LaB_6-W alloy sintered at 2070 K and 75vol%LaB_6-W sintered at

Table 3 Density of SPS sintered compacts of LaB_6-W.

Compositon	Sintering temperature(K)	Specific gravity	Relative density(%)
Pure W	1670	14.5	75
	1870	18.2	94
	2070	18.7	97
25vol%LaB6-W	1670	10.8	69
	1870	14.2	91
	2070	15.9	101
50vol%LaB6-W	1670	8.9	74
	1870	11.2	93
	2070	13.0	108
75vol%LaB6-W	1670	8.0	95
	1870	8.6	102
	2070	8.9	105

<Ideal density>
Pure W : 19.3
25vol%LaB6-W : 15.7
50vol%LaB6-W : 12.03
75vol%LaB6-W : 8.4

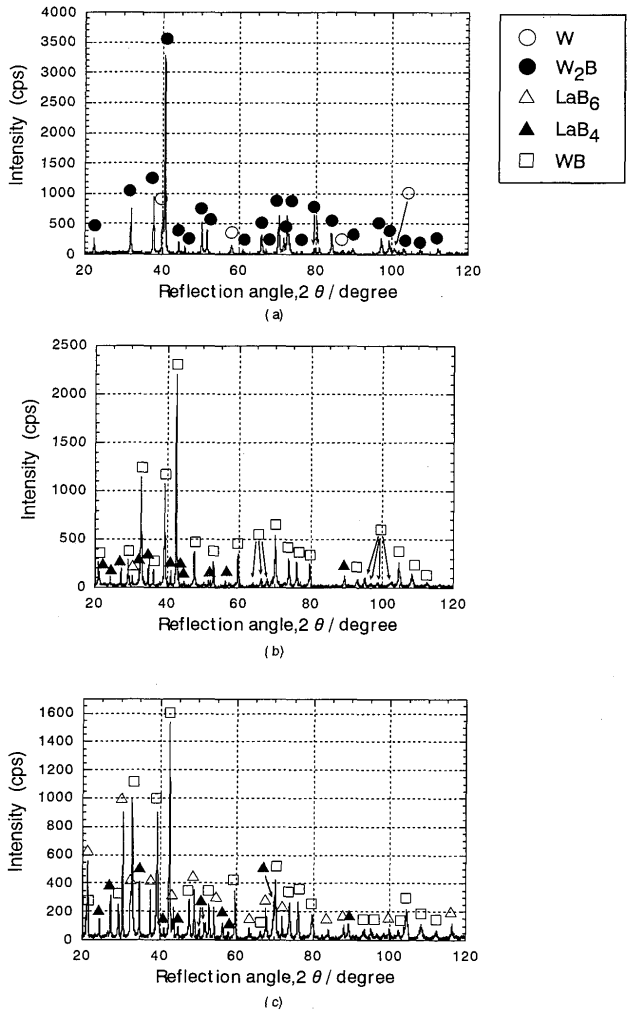

Fig. 2 XRD patterns derived from (a) 25vol%LaB_6-W, (b) 50vol%LaB_6-W, and (c) 75vol%LaB_6-W alloys sintered at 2070 K.

1870 K and 2070 K. These are the effect of reactions during sintering. LaB_6, a compound with comparatively low density (4.76 g / cm^3)[10], changed to other more dense compounds. This idea will be re-inforced with results from XRD and other metallographic analyses shown in the following section.

3. 2 Microstructure

XRD was conducted on each of 25vol%LaB_6-W, 50vol%LaB_6-W, and 75vol%LaB_6-W alloys sintered at 1670 K, 1870 K, and 2070 K. Interplanar spacings derived from reflections on diffraction patterns were compared with data in JCPDS cards, and corresponding phases were determined. Diffraction patterns from 25vol%LaB_6-W, 50vol%LaB_6-W, and 75vol%LaB_6-W alloys sintered at 2070 K are shown in **Fig. 2** (a), (b), and (c) respectively. In the diffraction pattern of 25vol%LaB_6-W, all the reflections observed were from W or ditungsten boride (W_2C), and there was no reflection corresponding to LaB_6. In the pattern from 50vol%LaB_6-W, Most of strong reflections were from Monotungsten Boride (WB), and there are some weak reflections from lanthanum tetraboride and faint ones from LaB_6. There was no reflection from metal W. In the pattern from 75vol%LaB_6-W, strong reflections from WB and LaB_6 were observed, and weak reflections from LaB_4 also. All the results from XRD are also summarized in **Table 4**. For standardisation, when peak intensity of the strongest reflection from one phase exceeded 1000 cps, that phase is represented by a double circle, phases of peak intensity from 200 to 1000 cps are represented by single circles, triangles are for phases of peak intensity under 200 cps, and X symbols are for phases not observed. For 25vol%LaB_6-W alloys observed reflections corresponded to W and W_2B, and for 50vol%LaB_6-W and 75vol%LaB_6-W reflections were from WB, LaB_4, and LaB_6, regardless of sintering temperature. These results show that, in every alloy reactions of W and LaB_6 should occur during sintering. In case of 25vol%LaB_6-W alloys, the reactions occurring can be expressed by the following formula

Table 4 Results from XRD measurements performed on SPS sintered LaB_6-W alloys.

Composition	Sintering temperature	Intensity of X-ray diffraction				
		LaB6	LaB4	WB	W2B	W
25%LaB6-W	1670 K	×	×	×	◎	○
	1870 K	×	×	×	◎	◎
	2070 K	×	×	×	◎	◎
50%LaB6-W	1670 K	△	○	◎	×	×
	1870 K	△	△	◎	×	×
	2070 K	△	△	◎	×	×
75%LaB6-W	1670 K	○	○	◎	×	×
	1870 K	○	△	◎	×	×
	2070 K	◎	△	◎	×	×

$$LaB_6 + 12W \rightarrow La + 6W_2B$$

and for 50vol%LaB_6-W and 75vol%LaB_6-W reactions can be expressed by the following formulae

$$LaB_6 + 2W \rightarrow LaB_4 + 2WB$$
$$LaB_4 + 4W \rightarrow La + 4WB.$$

So that W and LaB_6 in starting materials were exhausted respectively. If we now rewrite the compositions of starting materials by molar representation, and write formulae for reactions that should occur in alloys of each composition. Then:

25vol%LaB_6-W:
$$2LaB_6 + 27W \rightarrow 2La + 12W_2B + 3W$$

50vol%LaB_6-W:

$$8LaB_6 + 36W \rightarrow 5La + 3LaB_4 + 36WB$$

75vol%LaB_6-W:

$$4LaB_6 + 6W \rightarrow LaB_6 + 3LaB_4 + 6WB$$

Densities of alloys are calculated on the assumption that reactions of the above formulae finish completely during sintering and the generated compounds make perfectly dense compacts together. The calculated densities are compared with measured densities of the alloys sintered at 2070 K, and results are below:

	calculated	experimental
25vol%LaB_6-W:	15.83 g / cm^3	15.9 g / cm^3
50vol%LaB_6-W:	12.97 g / cm^3	13.0 g / cm^3
75vol%LaB_6-W:	8.78 g / cm^3	8.9 g / cm^3

Values used in calculation of density for the compounds are 4.76 (g / cm^3) for LaB_6, 5.39 (g / cm^3) for LaB_4, 6.15 (g / cm^3) for La, 19.3 (g / cm^3) for W, 17.1 (g / cm^3) for W_2B, and 15.7 (g / cm^3) for WB[10]. For all compositions, calculated values and experimental values show good agreement.

From these results, it is also important to note that it was not possible to restrain reactions of LaB_6 with W in the sintering process in spite of lowering the sintering temperature and time used in the SPS.

According to the formulae above, metal La should be generated through the reactions in 25vol%LaB_6-W and 50vol%LaB_6-W. However, no reflections from metal La was observed in diffraction patterns from alloys of those compositions.

In 50vol%LaB_6-W and 75vol%LaB_6-W, there was noticed a tendency that reflections from LaB_4 became weaker in diffraction patterns from alloys at higher sintering temperatures. This might be caused by decomposition of LaB_4 to LaB_6 and liquid La at high temperature.

Next we will show the results from optical microscopy and point analyses by EPMA.

In **Fig. 3** are shown optical micrographs of cross-sections of alloys sintered at 2070 K. Alloys in Fig (a), (b), and (c) are of compositions 25vol%LaB_6-W, 50vol%LaB_6-W, and 75vol%LaB_6-W, respectively. In the 25vol%LaB_6-W alloy, a major volume was occupied by silver-white polygonal crystal grains of several μm in diameter. The 50vol%LaB_6-W alloy was composed of round grains with

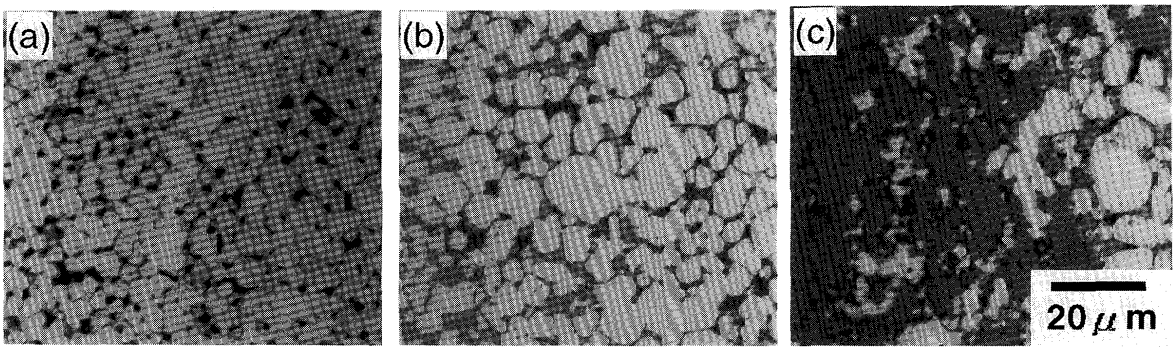

Fig. 3 Optical micrographs showing internal structures of (a) 25vol%LaB_6-W, (b) 50vol%LaB_6-W, and (c) 75vol%LaB_6-W alloys sintered at 2070 K.

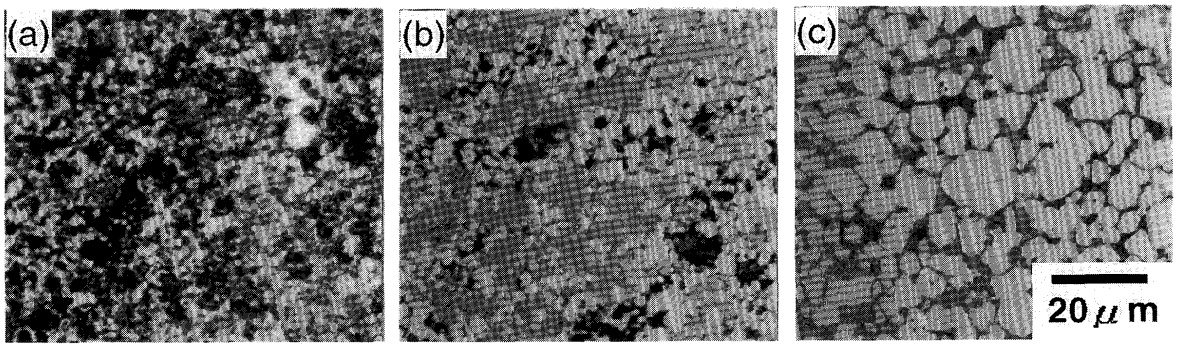

Fig. 4 Optical micrographs showing internal structures of 50vol%LaB_6-W alloys sintered at (a) 1670 K, (b) 1870 K, and (c) 2070 K.

diameters from 5 to 10 μm, appearing white in the photo, and grains appearing light gray filling spaces among the round grains. These two phases were also found in the 75vol%LaB_6-W alloy, and in that alloy there also existed grains appearing dark gray that occupied a rather large volume. This phase appeared vivid purplish red in color, it strongly suggests that this phase is LaB_6. This expectation is proved by results from EPMA later. Black areas of several μm in diameter seen in all photos are pores left after sintering.

In **Fig. 4** are shown optical micrographs of cross-sections of 50vol%LaB_6-W alloys. Fig. (a), (b), and (c) correspond to the alloys sintered at 1670 K, 1870 K, and 2070 K respectively. In alloys sintered at higher temperatures, volume fractions of pores became smaller, and mean size of crystal grains of each phase became larger.

Similar tendencies of change in microstructure with changes in composition and sintering temperature were observed in alloys of other compositions.

In order to identify compounds of phases observed by optical microscopy, crystal grains in some specimens were analyzed by EPMA. Results of analyses are shown for 25vol%LaB_6-W and 75vol%LaB_6-W alloys sintered at 2070 K in **Fig. 5** (a) and (b), respectively. In both figures, compositions at spots indicated by arrows in the SEM micrographs are given by corresponding numbers in the tables below the SEM micrographs. In the SEM image of the 25vol%LaB_6-W alloy, polygonal crystal grains were observed, similar to the in optical microscopy. It was shown that the main components of these grains were W and B (analyzed spots 5 and 6). Phases observed in the same 25vol%LaB_6-W alloy by XRD were W and W_2B, so these grains are confirmed as being W_2B. In the SEM image there were small white particles with diameters from 1 to 3 μm. Analyses of these particles (analyzed spots 1 and 4) and of black areas like pores (analyzed spots 2 and 3) show high concentration of La and oxygen (O), and small concentration of W . So these small particles are thought to be some oxide of La or a complex oxide of La and W, and the black areas are holes left after such particles separate from the matrix during polishing and etching. However, by XRD no trace of such oxide was observed, so a TEM observation of the same alloy was performed to determine the nature of these particles. We present those results later. In the 75vol%LaB_6-W alloy, there were round grains appearing white in the SEM image (analyzed spot 2, 4), and these

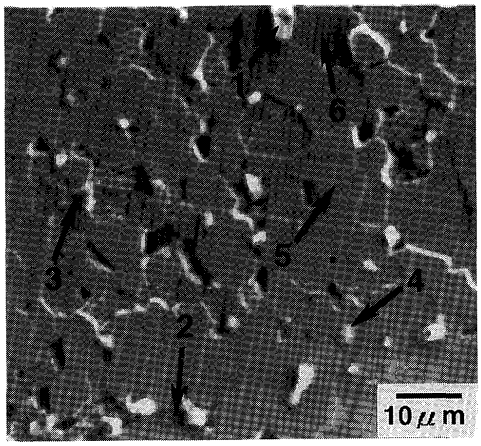

Analyzed spot	Concentraition (at%)			
	W	La	B	O
1	2	27	0	71
2	3	36	0	61
3	7	29	1	63
4	8	27	0	65
5	72	0	27	1
6	68	0	31	1

(a)

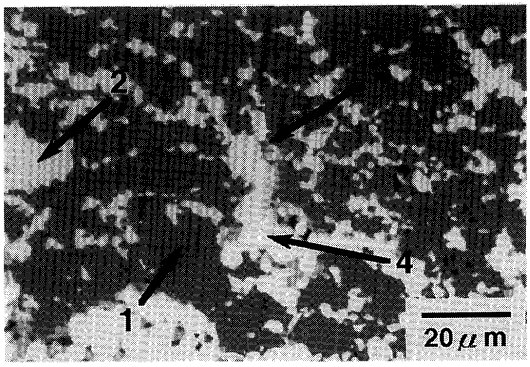

Analyzed spot	Concentration(at%)		
	W	La	B
1	0	14	86
2	64	0	36
3	0	19	81
4	58	1	41

(b)

Fig. 5 Results from EPMA point analyses of (a) 25vol%LaB_6-W and (b) 75vol%LaB_6-W alloys sintered at 2070 K. In both (a) and (b), SEM images are presented above, and compositions at spots pointed by arrows in SEM images are tabulated in tables below.

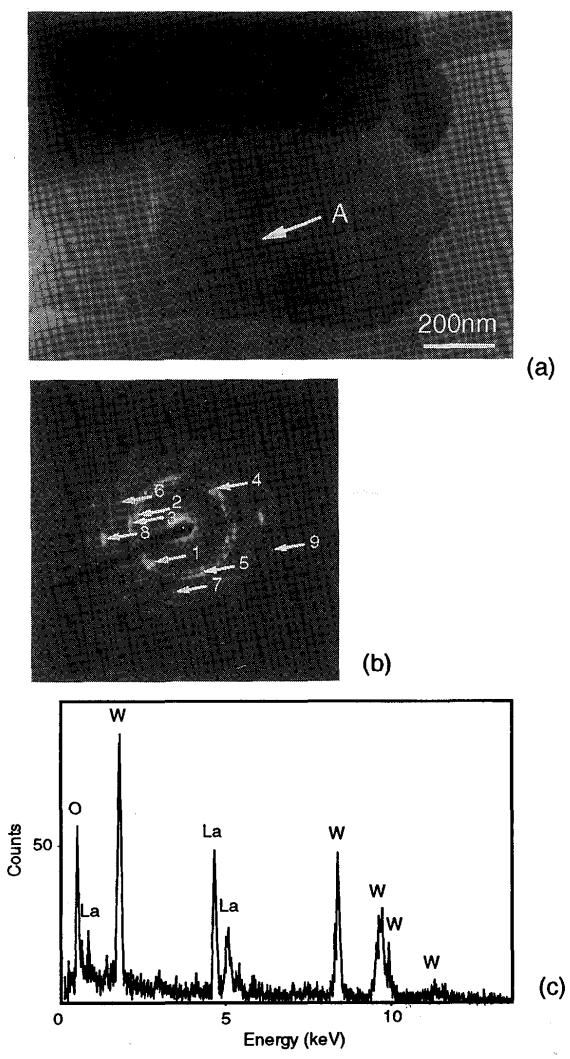

Fig. 6 Results from TEM observation of the 25vol%LaB_6-W alloy sintered at 2070 K. In (a) is shown the bright field image, and the SAED pattern and the EDS spectrum shown in (b) and (c) respectively were taken from thespot pointed by the arrow 'A' in (a).

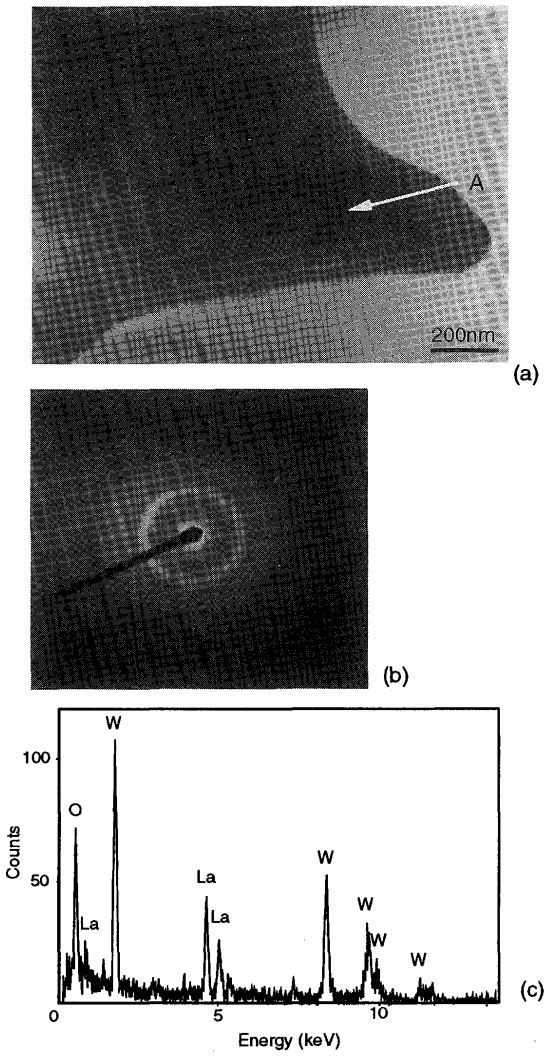

Fig. 7 Results from TEM observation of the25vol%LaB_6-W alloy sintered at 2070 K. In(a) is shown the bright field image, and theSAED pattern and the EDS spectrum shown in (b) and (c) respectively were taken from thespot pointed by the arrow 'A' in (a).

grains mainly consisted of W and B. So these grains were determined to be WB observed by XRD. In the same specimen there were grains appearing light gray (analyzed spot 3) and dark gray (analyzed spot 1), Both of these contained La and B. Phases that contain these two elements and observed in the same alloy by XRD were LaB_4 and LaB_6. Grains appearing light gray had more La concentration, therefore these are LaB_4, and grains appearing dark gray shall be LaB_6. Judging from size and shapes, correspondences of these three phases, WB, LaB_4, and LaB_6 to phases observed by optical microscopy are determined as follows: white round grains and light gray grains observed in 50vol%LaB_6-W and 75vol%LaB_6-W alloys are WB and LaB_4 respectively, and dark gray grains observed in 75vol%LaB_6-W is LaB_6.

In the last part of this section, we present results from TEM observation of 25vol%LaB_6-W alloy sintered at 2070 K.

In **Fig. 6** (a), (b), and (c) are shown a TEM micrograph, an SAED pattern taken from the region around the spot indicated by the arrow A in (a), and an EDS spectrum from the same spot A. On the EDS spectrum, there observed strong peaks of characteristic X-rays of W, La, and O. The result of analysis of the SAED pattern is given in **Table 5**. As shown in the table, interplanar spacings calculated from the pattern show good agreement with interplanar spacings of $La_2O_3 \cdot 2WO_3$, one of complex oxides of La and W, reported in JCPDS cards. The SAED pattern was what is called

Table 5 Results from analyses of the SAED pattern in Fig.6 (b). Interplanar spacings calculated from spots pointed arrows in Fig. 6 (b) are presented in the left column. In the right column are presented interplanar spacings of $La_2O_3 \cdot 2WO_3$ taken fromJCPDS cards.

Measured		JCPDS		
No.	d(nm)	La2O3 · 2WO3		
		d(nm)	hkl	I/Io
1	0.347	0.3490	/	40
2	0.341	0.3410	/	100
3	0.328	0.3230	/	60
		0.3120	/	75
4	0.302	0.3050	/	50
5	0.295	0.3000	/	70
		0.2838	/	30
		0.2557	/	30
6	0.223	0.2264	/	7
7	0.216	0.2174	/	4
8	0.197	0.1989	/	55

a 'necklace pattern', a pattern consisting of diffraction spots arranged in concentric circles. Such patterns indicate that the area from where the pattern was taken was polycrystalline. From these results, the area shown in the TEM image of Fig. 6 (a) is thought to have been an aggregate of nanocrystals of $La_2O_3 \cdot 2WO_3$. In **Fig. 7** are shown results from TEM observation of another place in the same specimen. The EDS spectrum shown in Fig. (c) had peaks of W, La, O like the spectrum in Fig. 6 (c), however, the SAED pattern on Fig. 7 (b) was a halo pattern without sharp diffraction spots or rings. So the area shown in the TEM image of Fig. 7 (a) should be a complex oxide of La and W similar to the area in Fig. 6 (a), and it was amorphous without definite crystal structure. These results show that La in 25vol%LaB_6-W alloys should exist as complex oxides with W, most of them being amorphous like the one observed in Fig. 7, because they could not be detected by XRD measurements.

3. 3 Discharge tests

The first, appearance of electrodes after discharge tests are shown in **Fig. 8**. Electrodes of 25vol%LaB_6-W, 2wt%La_2O_3-W, and carburized 2wt%La_2O_3-W had their tips un-melted and their changes in shape were small. On the other hand, electrode of 50vol%LaB_6-W showed rather large consumptions, moreover, electrodes of 75vol%LaB_6-W and pure LaB_6 changed their shapes considerably with melting of their tips. For these electrodes there are no data for discharging properties because their consumption during discharge was so great. Results for current vs. voltage characteristics will be shown for five specimens omitting these two.

Changes of discharging voltages with step by step changes of discharging currents are shown in **Table 6** and **Fig. 9** for each electrode. Electrode of 25vol%LaB_6-W showed the lowest discharging voltages among all the electrodes for most values of discharging current. The electrode of 50vol%LaB_6-W showed low discharging voltages in the early steps of the test, however, in the current decreasing cycle after maximum current value of 50 A it showed large increases of discharging voltages in comparison with steps

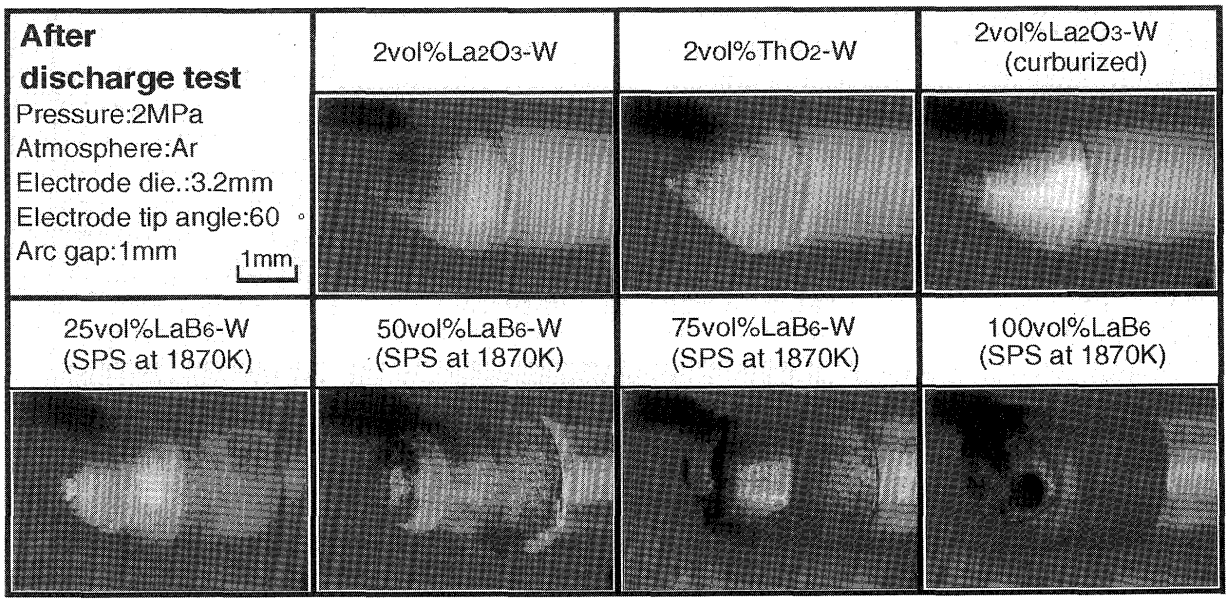

Fig. 8 Appearance of electrodes after discharge tests.

Table 6 Changes of discharging voltage with changes of discharging currents.

	2%La_2O_3-W	2%La_2O_3-W (+carburized)	2%ThO_2-W	25%LaB_6-W (SPS)	50%LaB_6-W (SPS)
↓ Current	Voltage(V)	Voltage(V)	Voltage(V)	Voltage(V)	Voltage(V)
10A	13.5	13.7	15.1	12.2	12.1
12A	13.6	13.5	14.8	11.3	11.2
15A	13.2	13.2	14.3	10.8	10.9
25A	12.4	12.4	13.3	11.4	11.9
40A	11.3	12.4	12.4	10.7	11.1
50A	11.8	12.5	12.9	11.0	11.4
40A	11.7	12.0	12.4	10.9	11.4
30A	12.1	13.3	13.2	11.7	13.1
25A	12.9	13.2	13.9	12.2	14.3
15A	15.0	14.2	15.0	13.1	20.0
12A	15.0	14.2	16.0	13.3	100.0
10A	15.0	14.6	17.0	14.3	100.0

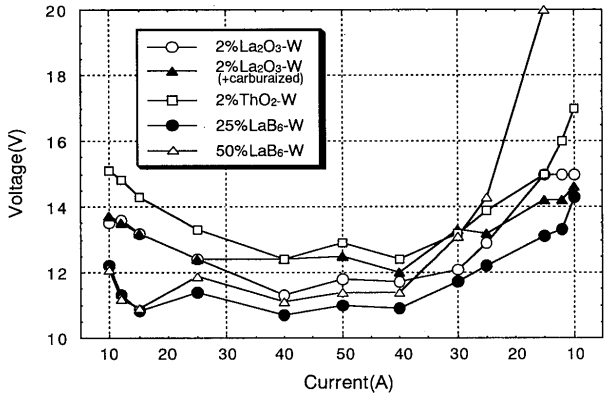

Fig. 9 Changes of discharging voltage with changes of discharging currents.

Table 7 Range of fluctuation of discharging voltage at each step of discharging currents.

	2%La_2O_3-W	2%La_2O_3-W (+carburized)	2%ThO_2-W	25%LaB_6-W (SPS)	50%LaB_6-W (SPS)
↓ Current	Voltage(V)	Voltage(V)	Voltage(V)	Voltage(V)	Voltage(V)
10A	0.20	0.90	0.10	0.20	0.20
12A	0.40	2.00	0.20	0.20	0.20
15A	0.80	0.60	0.20	0.40	0.20
25A	2.00	0.10	0.20	0.50	0.30
40A	0.50	0.30	0.60	0.05	0.05
50A	0.30	0.30	0.20	0.05	0.05
40A	0.30	0.30	0.80	0.05	0.20
30A	1.60	0.30	2.80	1.00	1.60
25A	2.40	0.50	0.90	0.60	8.00
15A	3.20	0.10	1.00	1.30	8.00
12A	5.60	0.50	1.80	1.30	8.00
10A	2.40	0.20	1.20	1.80	8.00

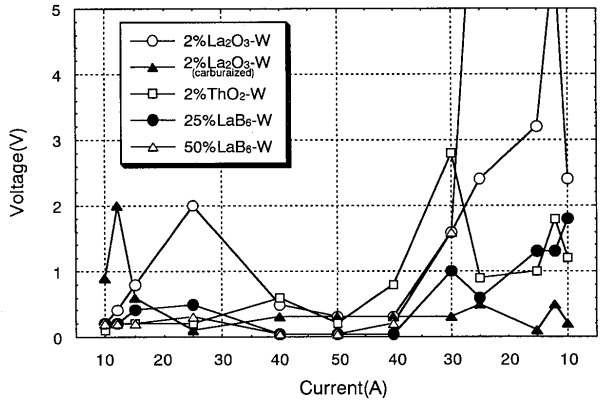

Fig. 10 Range of fluctuation of discharging voltage at each step of discharging currents.

of the same values of current in the former current increasing cycle. As expected from the appearance after the discharging test, the condition of the electrode of 50vol%LaB_6-W should change significantly during discharging through its consumption.

Ranges of fluctuation of discharging voltages at each step of discharging currents are shown in **Table 7** and **Fig. 10**. Electrodes of 25vol%LaB_6-W and carburized 2wt%La_2O_3-W relatively small fluctuation of discharging voltage all over the discharging currents.

As mentioned above, the 25vol%LaB_6-W alloy showed the best results from both the viewpoints of durability and stability of discharge among the LaB_6 doped alloys produced in this study. Electrodes of 50vol%LaB_6-W and 75vol%LaB_6-W suffered severe damage during discharging in spite of the fact that those alloys retained LaB_6 in them. It is suggested that one of the causes of the damage was the LaB_4 component of those alloys. The melting point of LaB_4 (2073 K) is rather lower than those of W (3673 K) and LaB_6 (2993 K)[10], so the 50vol%LaB_6-W and 75vol%LaB_6-W alloys that contains amounts of LaB_4 generated through decomposition of LaB_6 might not be able to resist the high temperature of discharging. On the other hand, in the 25vol%LaB_6-W alloy no LaB_6 left after sintering was observed by metallographic analyses, but that alloy showed rather good performance in discharging tests. A possible cause of this is the the existence of complex oxides of La and W in that alloy. Electrodes of La_2O_3 doped W used in the discharge tests for comparison also showed a good performance. Just like La_2O_3, complex oxides of La and W might work effectively as additives to improve thermo-electron emittance of the alloy. And W_2B itself, the major component of the 25vol%LaB_6-W alloy, is a material of high melting point (2800 K) and low work function (2.62 eV)[2], and these properties might exert good influences on performance as an electrode material.

4. Conclusions

LaB_6 doped W alloys were produced experimentally by spark plasma sintering. The alloys produced were analyzed metallographically, and discharge tests using electrodes made of these alloys were performed.

Results are summarized below:

(1) By SPS, dense sintered compacts of W alloys are available after 600 s at a sintering temperature of 2070 K. It

is a very rapid and low temperature process in comparison with conventional nonpressure Joule heating.

(2) In alloys produced by SPS, there were found several compounds generated by reaction between W and La, W_2B, WB, and LaB_4 according to the compositions of starting materials. In 25vol%LaB_6-W alloys, LaB_6 in the starting material were exhausted in reaction with W, and no trace was observed in the sintered compacts. In those alloys, La isolated through decomposition of LaB_6 was found forming complex oxides with W.

(3) In discharge tests, the 25vol%LaB_6-W alloy showed rather good properties among all the alloys produced in this study. Electrodes of 50vol%LaB_6-W and 75vol%LaB_6-W alloys suffered severe consumption during discharging. This may be caused by the LaB_4 component of those two alloys. Complex oxides and W_2B that the 25vol%LaB_6-W alloy contains may cause rather good performance of this alloy as an electrode material.

From these results, it can be said that, for development of new electrode materials, utilizing the functions of LaB_6, we should give more consideration to sintering condition and compositions of starting materials to restrain reactions of the components of the starting materials. The third result mentioned above shows a possibility of new electrode materials containing W_2B.

Acknowledgment

We express our great thanks to Toho Kinzoku K. K. for their kindly providing the specimen materials.

Refernces

1) A. A. Sadek: "Development of New Tungsten Electrode by Rare Earth Metal Oxide Additions for Inert Gas Arc Welding", Ph. D. thesis, 1989, Osaka University.
2) В. С. Фоменко: "Handbook of Electron Emittance (Denshi Hoshutsusei Benran)", Nisso Tsushinsha, 1970. (In Japanese)
3) Е. М. Савцчкций, В. Ф. Терехова: "Rare-Earth Metal (Kidorui Kinzoku)", Nisso Tsushinsha, 1975. (In Japanese)
4) K. Tanaka: "Fundamental Study on Development of Heat Cathode Materials for High Power Plasma Torches and Its Characteristics", Ph. D. thesis, 1996, Osaka University. (In Japanese.)
5) M. Tokita: Resent Movements of the Technology of SPS Spark Plasma Sintering (SPS Plasma-hoden-shoketsu no Saikin no Gijutsu Doko), Funtaikogakushi, vol. 30, no. 11, 1993. (In Japanese.)
6) T. Sakamoto: Sintering Behavior of Mo Powder Compact Applied SPS Spark Plasma Sintering Method, Funtai oyobi Funmatsuyakin Journal, vol. 44, no. 10, 1997, p.845 ~ 850. (In Japanese.)
7) N. Tamari et al: Effect of Spark Plasma Sintering on Densification, Material Properties and Cutting Performance of Titanium Carbide Whisker / Alumina Composite Ceramics, Journal of the Ceramic Society of Japan, vol. 105, no. 1226, 1997, p. 991 ~ 994.
8) A. Matsumoto, K. Kato, K. Andoh: Research and Development of Novel Materials by Plasma Discharge Sintering Process, Zairyo to Kankyo, vol. 44, no. 11, 1995, p.625 - 633. (In Japanese.)
9) Eds. T. Lyman: "Metals Handbook 8th Edition Vol.8 Metallography, Structures and Phase Diagrams", American Society for Metals, 1973.
10) Eds. R. Kubo et al: "Rikagaku Jiten 4th Edition", Iwanami Shoten, 1987. (In Japanese.)